Infrared Physics & Technology 90 (2018) 133–145

Contents lists available at ScienceDirect

Infrared Physics & Technology

journal homepage: www.elsevier.com/locate/infrared

Regular article

Spatial-time-state fusion algorithm for defect detection through eddy current pulsed thermography

Xiang Xiao [a], Bin Gao [a,*], Wai Lok Woo [b], Gui Yun Tian [a,b], Xiao Ting Xiao [a]

[a] School of Automation, University of Electronic Science and Technology of China, China
[b] School of Electrical and Electronic Engineering, Newcastle University, England, UK

HIGHLIGHTS

- Spatial-time-state Fusion strategy for unsupervised defects detection by state Eddy Current Pulsed Thermograph.
- Genetic algorithm and new fitness function are embedded for automatically feature selection.
- Common defect detection methods have been conducted for comparison.

ARTICLE INFO

Article history:
Received 2 November 2017
Revised 24 February 2018
Accepted 28 February 2018
Available online 9 March 2018

Keywords:
Eddy current pulsed thermography
Independent component analysis
Common orthogonal basis extraction
Genetic algorithm

ABSTRACT

Eddy Current Pulsed Thermography (ECPT) has received extensive attention due to its high sensitive of detectability on surface and subsurface cracks. However, it remains as a difficult challenge in unsupervised detection as to identify defects without knowing any prior knowledge. This paper presents a spatial-time-state features fusion algorithm to obtain fully profile of the defects by directional scanning. The proposed method is intended to conduct features extraction by using independent component analysis (ICA) and automatic features selection embedding genetic algorithm. Finally, the optimal feature of each step is fused to obtain defects reconstruction by applying common orthogonal basis extraction (COBE) method. Experiments have been conducted to validate the study and verify the efficacy of the proposed method on blind defect detection.

1. Introduction

Non-destructive testing (NDT) refers to a wide group of analysis techniques used in industry to evaluate the properties of a material, component or system without causing damage [1,2]. Conventional NDT methods include X-ray detection, ultrasonic testing, magnetic particle testing and eddy current testing [3]. Stress concentration and superficial cracks inevitable exist in mechanical parts during the manufacturing and in service process. This leads to considerable hazards in industrial activities. Therefore, the detection of cracks is important [4].

Magnetic Particle Testing (MT) [5] is effective for the detection of surface and near-surface discontinuities while it has a complicated detecting procedure. The surface of the sample requires pretreatment and the detection time is relatively long. Moreover, MT produces pollution. Penetrant Testing (PT) [6] is sensitive to open surface cracks. Unfortunately, the surface coating significantly affects the detection rate that leads to ineffective inspection for fatigue cracks. Alternatively, the electromagnetic method has been widely used for the inspection of surface/subsurface flaws. Alternating Current Field Measurement (ACFM) has been proven to be effective in detecting surface breaking geometrical defects in any direction under simulation [7].

In recent years, with the rapid development of thermal imaging equipment, infrared thermography (IT) based NDT has been used for composite defect detection and cracks identification among others. It has several promising advantages [8,9] such as rapid inspection over a large region, non-contact and high sensitivity.

Eddy Current Pulsed Thermography (ECPT) is a multi-physics coupling method. The combination of eddy currents heating and thermal diffusion is beneficial for detecting turbulence in conductive materials by analyzing the thermal patterns [10]. Eddy current pulsed thermography combines the advantages of pulsed eddy current (transient analysis and eddy current interpretation) and merits of thermography (fast and high resolution), which has been widely used for damage detection in metallic alloy [11]. Recently, ECPT has been used in many defects detection applications such as crack detection of carbon fiber reinforced plastic materials, compressor blades, and fatigue cracks [12,13]. In addition, the relevant

* Corresponding author.
E-mail address: bin_gao@uestc.edu.cn (B. Gao).

https://doi.org/10.1016/j.infrared.2018.02.012
1350-4495/

signal processing methods have been proposed in ECPT. He et. al. used time to peak feature for wall thinning and inner defects characterization [14]. However, the transient response features always suffer from noise. In order to enhance the contrast between the defects and the noise, patterns-based processing methods have been proposed. These include Principal Component Analysis (PCA), Independent Component Analysis (ICA) and sparse decomposition. PCA was used to extract an orthogonal thermography features by compressing the initial video sequences instead of analyzing each image [15]. Bai et. al. [16] proposed ICA to highlight the anomalous patterns of ECPT for crack identification in metallic specimen. Nedeljko Cvejic et. al. [15] presented a novel region-based multimodal image fusion algorithm in the ICA domain. Gao et. al. reported blind source separation algorithm on ECPT for automatic crack detection and identification [17].

In order to increase the effective detection area and enhance the accuracy of detectability, the fusion methods are suitable candidates in NDT applications. Canonical Correlation Analysis(CCA) is proposed for information fusion. The purpose of CCA is to identify and quantify the relationship between two sets of variables. The focus is on the correlation between a linear combination of one set of variables and a linear combination of the other set of variables. It can be used for feature fusion. Pan et. al. applied CCA for information fusion, which laid the mathematical foundation. In addition, CCA was used in pattern recognition, which implements the feature-level fusion [18]. However, CCA mainly solves the problem of correlation between two multivariate random vectors whereas it cannot solve the problem of fusion between multiple data. Zhou et. al. [19] proposed a new framework for common and individual feature extraction (CIFE) which identifies and separates the common and individual features from the multiblock data. Gao L et. al. [20] proposed a novel approach for multi-feature information fusion based on the Discriminative Multiple Canonical Correlation Analysis (DMCCA), which can extract more discriminative characteristics for pattern recognition. Rasha Ibrahim et. al. [21] presented a pixel-level image fusion technique based on integrating the sparse representation with robust principle component analysis algorithm (RPCA) to promote relevant information, eliminate noise and preserve edges.

At the present stage, although signal processing technology has made progress in ECPT analysis, it has encountered many practical issues. Current detection methods are mostly established where the location of cracks is assumed known a priori. In real applications, the position of defects is almost unknown. Thus, it becomes necessary to be able to detect cracks by directional scanning.

In this paper, a feature-level fusion method is proposed and applied to state the effect of ECPT on the treatment of surface cracks for metal material. Unlike the above general model, the proposed method allows automated reconstruction of the defect region as well as suppression of the interference background so that the defects can be detected without knowing prior knowledge. In addition, the proposed model can significantly improve the defect detection precision and this will be demonstrated on artificial and natural steel cracks. The remainder of this paper is organized as follows: Firstly, the introduction of ECPT system and the proposed method are presented in Section 2. The results and discussions are presented in Section 3. Finally, conclusions and further work are outlined in Section 4.

2. Methodology

2.1. Introduction of state ECPT system

Fig. 1 shows the diagram of state ECPT NDT&E system. According to the law of electromagnetic induction, when alternation current is driven into induction coil, the conductor near the coil generates an induced eddy current. When eddy current encounter a defect, the vortex will be forced to bypass the defect and results in eddy density increasing or decreasing in part of regional. Thus, the heat generated by the conductor will appear unevenly distributed, and the distribution of the surface temperature is recorded by infrared camera [22].

Using the Joule's law to couple the eddy current field and the temperature field [23], the heating power (internal heat source density or intensity) generated by the induced eddy current in the specimen is denoted byQ, namely

$$Q = \frac{1}{\sigma}|J_e|^2 = \frac{1}{\sigma}|\sigma E|^2 \quad where\ \sigma = \frac{\sigma_0}{1+\alpha(T-T_0)} \tag{1}$$

In general, by taking account of heat diffusion and Joule heating, the heat conduction equation of a specimen can be expressed as:

$$\frac{\partial T}{\partial t} = \frac{k}{\rho C_p}\left(\frac{\partial^2 T}{\partial x^2}+\frac{\partial^2 T}{\partial y^2}+\frac{\partial^2 T}{\partial z^2}\right)+\frac{1}{\rho C_p}q(x,y,z,t) \tag{2}$$

where $T = T(x,y,z,t)$ is the temperature distribution, k is the thermal conductivity of the material (W/m K), which is dependent on temperature. ρ is the density (kg/m3), C_p is specific heat (J/kg K). $q(x,y,z,t)$ is the internal heat generation function per unit volume, which is the result of the eddy current excitation. From the above analysis, it becomes clear that the variation of temperature spatially and its transient response recorded from the IR camera directly reveals the intrinsic properties variation of the conductive material. Through the analysis of thermal image, it becomes clear that the variation of temperature spatially and its transient response recorded from the IR camera directly reveals the intrinsic properties variation of the conductive material.

The pulse generator transmits signals to IR camera and induction heater simultaneously. The induction heater generates an electromagnetic and thermal field on the conductive specimen. With the continuous movement of the inductor, the IR camera will record the video of each state termed as $\mathbf{V}_n \in R^{N_x \times N_y \times J_n}$, where N_x, N_y denote the length and the width of each image frame in the thermal video, respectively. $J_n n \in \{1,2,\ldots,N\}$ denotes the total number of frame for each state.

2.2. Strategy

The specific procedure of the proposed fusion strategy (as shown in Fig. 2) consists of: firstly, thermal video sequences under different states are obtained by directional scanning. Secondly, features extraction using ICA and genetic algorithm embedded for automatically selecting the defect related ICA components for each state. Finally, COBE is conducted for the fusion procedure. The following sections will present the proposed method. It should be noted that all the parameters set in this work have been validated by Monte Carlo based experiment approach where the process is repeated over 10 realizations.

2.3. ICA for feature extraction

ICA [24] has the capability to automatically extract valuable spatial and time patterns according to the whole transient response behavior. Here, the number of features separated by ICA is set as M.

In order to facilitate the calculation of ICA, three-dimensional tensor will be converted into a two-dimensional matrix. Single frame of the thermal video $\mathbf{V}_n \in R^{N_x \times N_y \times J_n}$is sorted by vectorizing each frame, namely $\mathbf{Y}_n(t) \in R^{D \times J_n}$, where $D = N_x \times N_y$. $\mathbf{Y}_n(t)$ can be considered as a mixing observation. $\mathbf{X}_{nm}(t)$ is considered as thermal

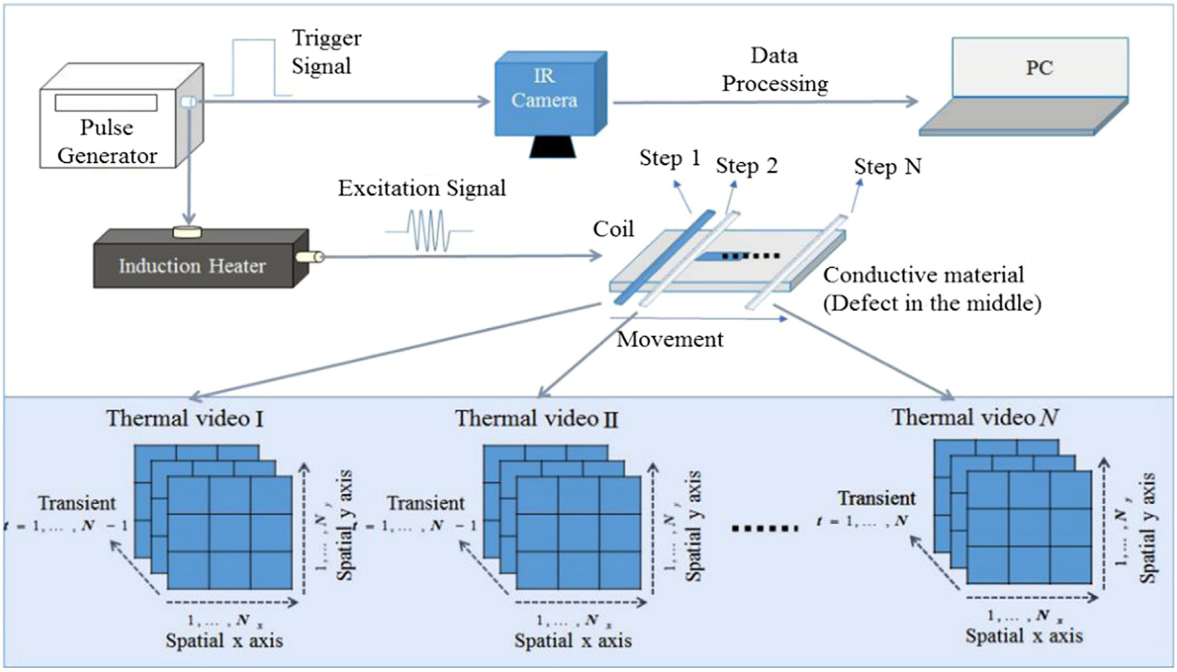

Fig. 1. State ECPT schematic diagram.

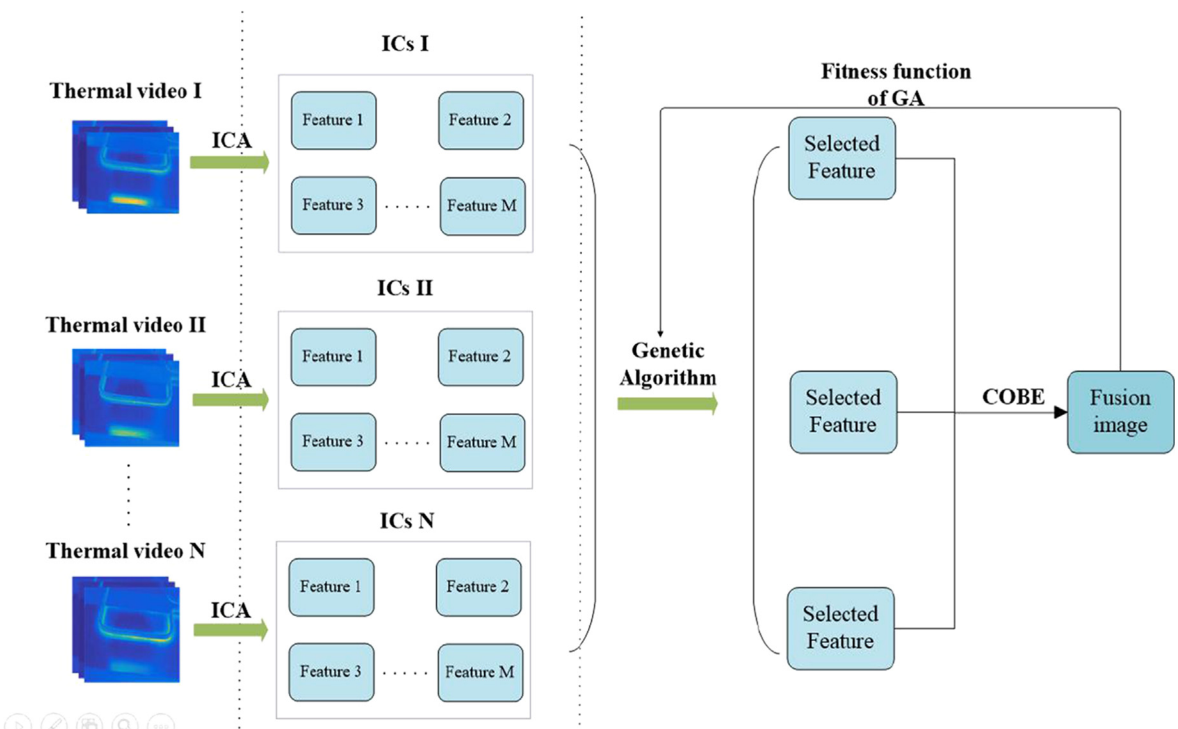

Fig. 2. Proposed fusion strategy.

pattern in which the regions of features are with different spatial and time distribution, namely independent components. The term m stands for the feature serial number separated by ICA $(m = 1, 2, \ldots, M)$ and $\mathbf{w}_m$the mixing parameter. $\mathbf{Y}_n(t)$ can be considered as a linear instantaneous mixing model given by

$$\mathbf{Y}_n(t) = \sum_{m=1}^{M} \mathbf{w}_m \mathbf{X}_{mn}(t) \quad n = 1, 2, \ldots, N \tag{3}$$

where $\mathbf{X}'_{mn}(t) = [\mathrm{vec}(\mathbf{X}_{1n}(t)), \mathrm{vec}(\mathbf{X}_{2n}(t)), \ldots, \mathrm{vec}(\mathbf{X}_{Mn}(t))]^T$ and $(\mathrm{vec}(\mathbf{X}_{mn}(t))m = \{1, 2, \ldots, M\}$. The ICA learning algorithm is equivalent to searching for the linear transformation that make the components as statistically independent as possible, as well as maximizing the marginal densities of the transformed coordinates for the given training data. This can be performed by using fixed point iteration algorithm to estimate $\mathbf{X}'_{ICA} = \mathbf{W}^{-1}_{ICA}\mathbf{Y}'$, the specific steps of approach for thermal pattern separation by using ICA can be found in [25] and [26].

2.4. GA for features selection

Genetic Algorithm is firstly proposed by Holland which has been used to trace the procedure of evolution of stochastic global parallel search [27]. It has the advantages of strong robustness and global optimization performance. Because in each step most of the features separated by ICA contain fewer defect information, it is necessary to find out the feature which contains the most defect information. Here the genetic algorithm is used for features extraction.

In inductive thermography, if defect exists, the distribution of eddy current (EC) or the process of thermal diffusion will be disturbed. Therefore, in the heating stage, different areas have different heat generation rates which subsequently lead to temperature spatial variation. Hot spots are mainly distributed around the crack tips. Follow this mechanism, the strategy is to select the mean of top H (e.g. $H = 100$) highest temperature points as the representative of relevant defect regions. Specially, the defects caused of temperature rising region are relatively small, the background temperature can be considered to be the average of the temperature of the entire fused image. Thus, in order to enhance the contrast between defective and non-defective areas, the appropriate fitness function for thermal features selection should be generated and this can be calculated as follow:

$$\max f = \frac{avg\left(\sum_{i=1}^{H}\mathbf{T}_i\right)}{avg\left(\sum_{i=1}^{S}\mathbf{T}_i\right)} \tag{4}$$

where $\mathbf{T}$ represents the vector of the fused image in descending order intensity. S represents the number of elements of the entire fused image.

The significance of the cost function lies in the ability to extract features better, especially for single cracked video. We assume that H is the number of pixels in the crack, and H is set to 100. In this way, it can guarantee that the crack information is continuously enhanced through the multi-step fusion when there is a crack (usually a crack contains more than 100 pixels). When a pixel in the same position fuses at different steps, the larger the pixel value in the feature is, the larger is the pixel value in the fusion image. If a feature does not contain the top H largest pixel information points, it will choose the feature which contains fewest thermal information feature to make $avg(\sum_{i=1}^{S}\mathbf{T}_i)$ as small as possible. The result is that genetic algorithm continues to find features that enhance the information of a crack.

Table 1 and Fig. 3 give the specific parameters and flowchart of genetic algorithm, respectively. In the first stage of the proposed method, all individuals of the population were initialized. The feature number extracted from each step was randomly selected by binary encoding and subject to gene coding. In the second stage, each individual was decoded and carried out by applying COBE fusion model and its fitness function was computed. In the third stage, it will conduct tournament selection, single-point crossover and mutation operations to generate new offspring population. In the fourth stage, the procedure repeats the second and third stages until the function converges. Finally, COBE fused image will be generated by the proposed embedded genetic algorithm.

Table 1
GA parameters used for features selection.

Coding type	Binary coding
Population Size	30
Selection type	2-tournament selection
Crossover type	Single-point crossover
Mutation type	Uniform
Crossover probability	0.6
Mutation probability	0.01
Maximum number of iterations	10

2.5. COBE for features fusion

In the detection of directional scanning of each state, although the heat abnormality will be concentrated in the defect while noise is being generated. The noise is greatly influenced by the coil and the test environment. Thus, features fusion should not only suppress the noise but also reconstruct the full profile of the defects. In this paper, common orthogonal basis extraction (COBE) method is used for the features fusion. COBE can extract common basis that characteristic is shared by all blocks of data. Comparing with the traditional features fusion algorithm such as principal component

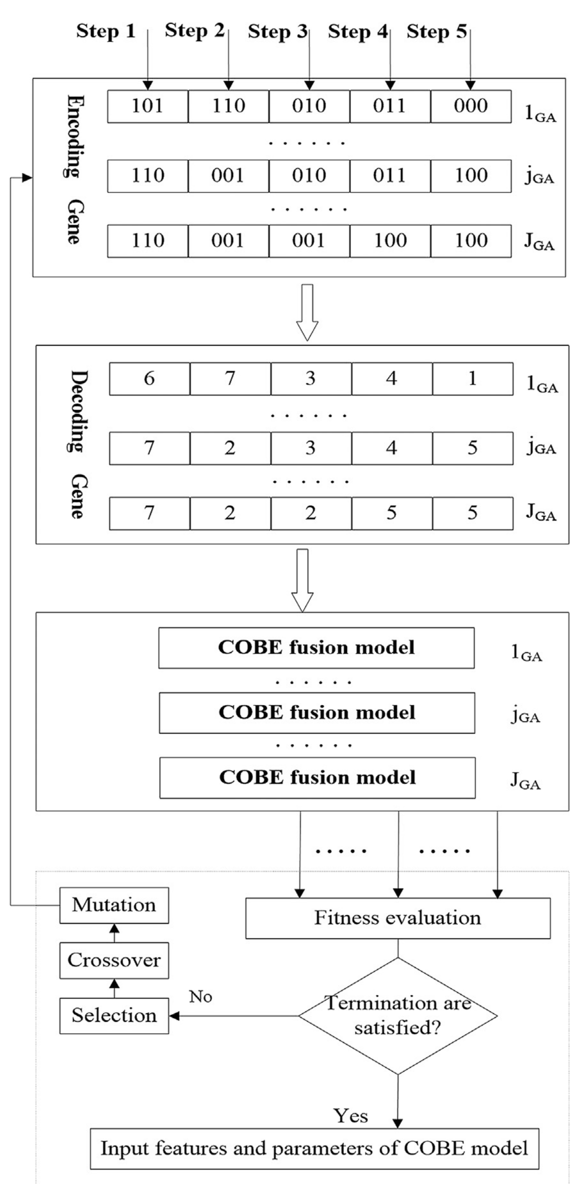

Fig. 3. Flowchart of the proposed embedded genetic algorithm.

analysis (PCA), canonical correlation analysis(CCA) [28], COBE offers several potential advantages.

1. COBE can identify real common subspace even if the common components are relatively weak.
2. The time complexity of COBE algorithm is relatively low as it is convenient to carry on the iteration of genetic algorithm.
3. PCA focuses on the "decentralized" information of the variables, while CCA is based on the identification and quantification of the statistical relevance of the two sets of variables, which is the promotion of the correlation from two random variables to two sets of variables. COBE extracts only components for which the correlation is higher than a specified threshold.

The detailed description of COBE on the proposed structure is specified as follows.

Consider a set of ICA components of ECPT for all states $y = \{\mathbf{Y}_n \in R^{D\times J_n} : n \in S\}, S = \{1, 2, \ldots, N\}$ obtained by directional scanning. A matrix decomposition problem is involved whereby for each matrix $\mathbf{Y}_n \in y$, we seek:

$$\min \|\mathbf{Y}_n - \mathbf{A}_n\mathbf{B}_n^T\|_F^2, n \in N \tag{5}$$

where the R_n columns of $\mathbf{A}_n \in R^{D\times R_n}$ represent the latent variables in $\mathbf{Y}_n$, and $\mathbf{B_n} \in R^{J_n\times R_n}$ denotes the corresponding coefficient matrix. The matrix product $\mathbf{A_n}\mathbf{B}_n^T$ provides a compact/compressed or low-rank representation of Y_n .

Let $\mathbf{A}_n = \left[\overline{\mathbf{A}}\, \widetilde{\mathbf{A}}_n\right]$, $n \in N$ where $\overline{\mathbf{A}} \in \mathbf{R}^{\mathbf{D}\times\mathbf{1}}$, $\widetilde{\mathbf{A}} \in R^{D\times(R_n-1)}$, we assume the common component vector $\overline{\mathbf{A}}$ contains the common components shared by all the matrices, while the submatrix $\widetilde{\mathbf{A}}$ contains the individual information. The decomposition of the matrix can be approximated as follows:

$$\mathbf{Y}_n \approx \mathbf{A}_n\mathbf{B}_n^T = \begin{bmatrix}\overline{\mathbf{A}} & \widetilde{\mathbf{A}}_n\end{bmatrix}\begin{bmatrix}\overline{\mathbf{B}}_\mathbf{n}^\mathbf{T} \\ \widetilde{\mathbf{B}}_n^T\end{bmatrix} = \overline{\mathbf{A}}\overline{\mathbf{B}}_\mathbf{n}^\mathbf{T} + \widetilde{\mathbf{A}}_\mathbf{n}\widetilde{\mathbf{B}}_\mathbf{n}^\mathbf{T} \tag{6}$$

Table 2
The description of different samples.

Sample	Indication	Dimension	Defect information	Picture
Sample(a)316# stainless steel	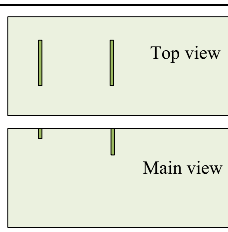	120 × 60 × 6 (mm)	2 types of cracks with different depth (8 × 0.5 × 0.5, 8 × 0.5 × 1.2(mm)) notches are manufactured	
Sample(b)316# stainless steel	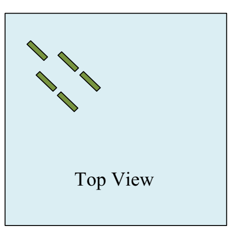	130 × 130×10 (mm)	5 45°-angle man-made cracks (8 × 0.1 × 1(mm))	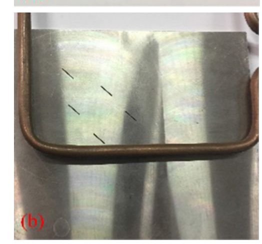
Sample(c)45# steel	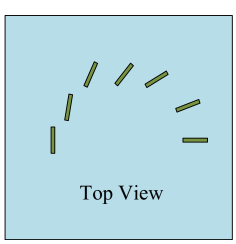	130 × 130 × 10 (mm)	Different angle cracks (0°, 15°, 30°, 45°, 60°, 75°, 90°), the cracks size are all 8 × 0.1 × 1(mm)	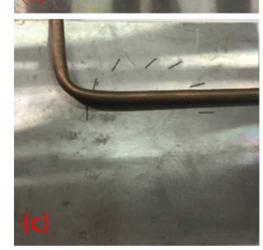
Sample(d)316# stainless steel	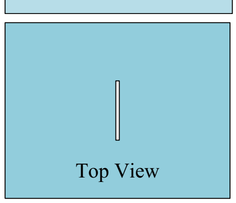	200 × 100 × 18 (mm)	A long natural crack	
Sample(e)railway	Dozens of natural fatigue cracks	115 × 7 × 180(mm)	Many natural cracks	

where $\overline{\mathbf{B}}_\mathbf{n}$ and $\widetilde{\mathbf{B}}_n$ are the partitions of the coefficients $\mathbf{B_n}$ that corresponding to $\overline{\mathbf{A}}$ and $\widetilde{\mathbf{A}}_n$. Let $\mathbf{Y}_n = \mathbf{U}_n\mathbf{H}_n$, $\mathbf{U}_n$ is extracted by $\mathbf{Y}_n$ through ICA. $\mathbf{U}_n$ is an orthogonal vector, $\mathbf{U}_n^T\mathbf{U}_n = \mathbf{I}$and $\mathbf{Z}_n = \mathbf{H}_n\mathbf{B}_n^{T\dagger}$, $(\cdot)^\dagger$represents the Moore-Penrose matrix pseudoinverse.

Thus, the common components can be estimated by solving:

$$\min_{\mathbf{Z_n},\overline{\mathbf{A}}}\sum_{n=1}^{N}||\mathbf{U}_n\mathbf{Z}_n - \overline{\mathbf{A}}||_F^2,\ s.t.\ \overline{\mathbf{A}}^\mathbf{T}\overline{\mathbf{A}} = \mathbf{I} \tag{7}$$

$$\min_{\bar{\mathbf{a}},\mathbf{Z_n}} f = \sum_n ||\mathbf{U}_n\mathbf{Z}_n - \bar{\mathbf{a}}||^2,\ s.t.\ \bar{\mathbf{a}}^T\bar{\mathbf{a}} = \mathbf{1} \tag{8}$$

Among them, $\mathbf{U}_n$ is known as the ICA component, the common components of the interested $\bar{\mathbf{a}}$can be obtained by continuous iteration. Finally, reshape $\bar{\mathbf{a}}$to get the fusion image of multi-step thermal video data.

The overall algorithm flow of the proposed method is shown below:

Input: $y = \{\mathbf{Y}_n \in R^{D\times J_n} : n \in S\}, S = \{1, 2, \ldots, N\}$ thermal videos obtained by IR camera, all state videos, ε correlation coefficient threshold
Initialization: $\mathbf{ICA}_{nm} m = \{1, 2, \ldots, M\}$ is the ICA decomposition of $\mathbf{Y}_n$
Output: Fusion image with the highest fitness value $\bar{\mathbf{a}}$
Initialize population P
for i = 1 to max_iteration
  compute the fitness value{
    while (f<ε)
      $\bar{\mathbf{a}}_\mathbf{i} = \sum_\mathbf{n}\mathbf{ICA_{nm}Z_n}/\|\sum_\mathbf{n}\mathbf{ICA_{nm}Z_n}\|_\mathbf{F}, \mathbf{n} \in \mathbf{N}, \mathbf{m} \in \mathbf{M}$
      $\mathbf{Z}_n = [\mathbf{ICA}_{nm}]^T\bar{\mathbf{a}}_\mathbf{i}$
    end (stop condition)
    $f = \frac{avg(\sum_{i=1}^{H}\mathbf{T}_i)}{avg(\sum_{i=1}^{S}\mathbf{T}_i)}$, The T vector is obtained by arranging the value of $\bar{\mathbf{a}}_\mathbf{i}$ in descending order
}
  select parents $p_j, j = \{1, 2, \ldots, |\mathbf{P}|\}$ from P by fitness value
  offspring = crossover (p_1, p_2)
  mutation(offspring)
  replace P with offspring
  return $\bar{\mathbf{a}}_\mathbf{i}$
end (stop condition)

---

3. Result and discussion

3.1. Sample preparation and experiments setup

In order to validate the robustness of the proposed method, a large number of experimental tests were conducted. The experiments contain a variety of test samples including ferromagnetic material (45# steel) samples with artificial cracks, non-ferromagnetic material (316# stainless steel) samples with artificial cracks, ferromagnetic material (steel rails) samples with natural cracks and non-ferromagnetic material (316# stainless steel) samples with natural cracks. Table 2 gives a comprehensive description of the samples [29,30]. These samples are all metal specimens containing cracks.

The experimental set-up is shown in Fig. 4. An Easyheat 224 from Cheltenham Induction Heating is used for coil excitation. The Easyheat has a maximum excitation power of 2.4 Kw, a maximum current of 400 A_{rms} and an excitation frequency range of 150–400 kHz (380 Arms and 256 kHz are used in this study). Water cooling of the coil is implemented to construct direct heating of the coil [31]. The IR camera, A655SC is a Stirling un-cooled camera with InSb detectors of 640 × 480 array, and the camera has a sensitivity if ≤50 mK. In the experiment, only one edge of the rectangular coil is used to stimulate eddy current to the underneath sample, and placed in the middle of the crack. In this study, the frame rate of 100 Hz is chosen, and 200 ms videos are recorded in the experiments.

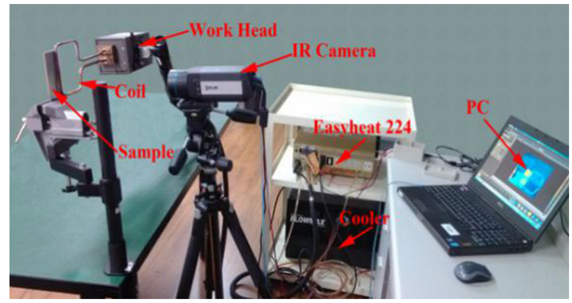

Fig. 4. Experiment setup.

Since these samples are all metal specimens, they have a relatively large conductivity. According to skin depth calculation formula

$$\delta = \frac{1}{\sqrt{\pi\mu\sigma f}} \tag{9}$$

where f is the frequency of excitation signal, σ is the electrical conductivity (S/m), and μ is the magnetic permeability (H/m). For metal materials with great conductivity and permeability, the skin depth is very small on the order of micrometers and the heating style is surface heating. For volume heating, ECPT also has a good effect on the composite materials with smaller conductivity [32].

All experiments are set with proper steps to minimize the influence. In addition, as ECPT has the characteristic of local volume induction heat that leads to the penetration of the subsurface on the sample by ways of eddy current penetration. Therefore, the reflection/shadow effect is limited. All these guarantee the effectiveness of the experimental data.

3.2. B. Results analysis

3.2.1. Multi-step fusion versus single-step detection

In this section, the significance of multi-step fusion method is required to be verified. The main significance of the multi-step fusion over single-step detection can be drawn as follows (1) detection area of the single-step detection is limited, (2) single-step detection cannot reconstruct the whole profile of defect and (3) failed detection without knowing prior knowledge of the crack position. Take sample (d) as an example.

In Fig. 5, the coil has moved in step-by-step. The infrared camera records the thermal video sequence in each step. Different components by ICA would be separated from the thermal video sequence. Here, the number of steps and the total number of features are both set as 4. Therefore 16 single-features can be obtained by ICA.

The proposed method judges the pros and cons through the effective pixels at the defect region. Effective pixels refer to pixels belonging to both high temperature area and defective area. A pixel is not only in high temperature area (this is based on the threshold of the fusion image), but also in the defective area (this is based on the prior information). For example, in Fig. 6, we determine that the red box is defect area through prior information (the crack position which has already been confirmed by using other NDT techniques, e.G. magnetic particle). However, this region is still

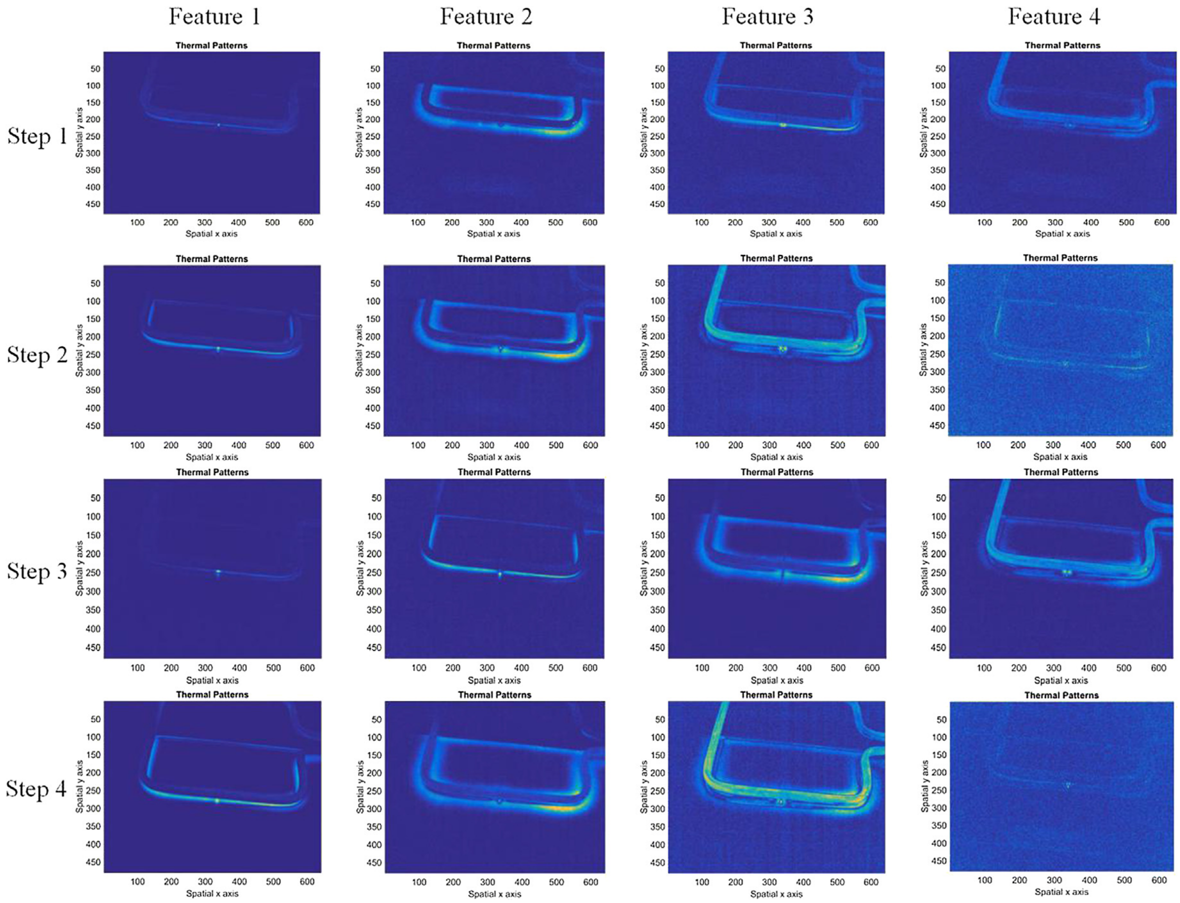

Fig. 5. The features of Sample (d) extracted by ICA.

too large that it cannot exactly represent the crack area. Indeed, the crack area is marked with the white box, Thus, the specific approach is to take a threshold in the red box area and the pixel which is above the threshold is considered as an effective pixel.

The effective pixels for all features of Fig. 5 are calculated, and Fig. 7(a) shows the feature which contains the most effective pixels in Fig. 5 that represent the defect. Due to the limitations of the excitation area by coil, one step detection cannot cover all specimen, and the occlusion of coil. The number of effective pixels is only 71. In Fig. 7(b), it is obtained by the proposed fusion method and the number of effective pixels is 154. The number of effective pixels of the fusion image is twice as large as the best single-step feature. It validates that fusion based strategy is better than the single-step detection.

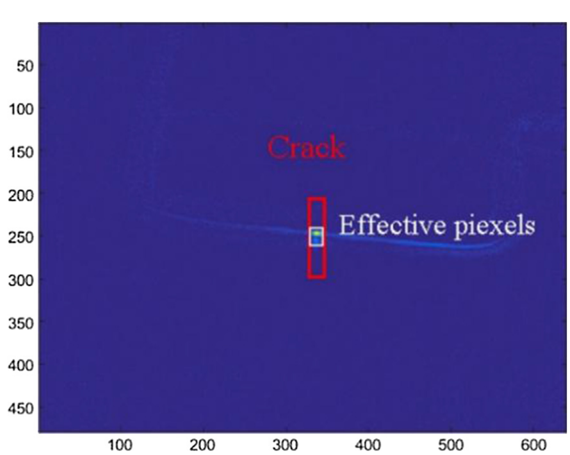

Fig. 6. A feature extracted by ICA for sample (d).

3.3. Comparison of different fusion strategy

3.3.1. Linear weighting method

The linear weighting method simply obtains the mean of all thermal video sequences. Assuming that the fused g (g is the result of vectorization of the linear weighted images), it can be obtained by the following formula

$$g = mean_Y\left(\sum_{n=1}^{N}\mathbf{Y}_n\right)/N \qquad (10)$$

where $mean_Y$ represents the mean of all rows of the matrix.

In comparison, the advantage of the linear weighting fusion strategy is not relying on the feature extraction and therefore no information will be loss from this fusion. However, because the feature extraction is not carried out, it will cause excessive noise and results worse detection rate.

3.3.2. Skewness method

The importance of features selection has been described earlier. Here, the selection of features by skewness method also confirms the feasibility.

Non-Gaussian refers to the symmetry of a random variable probability distribution, which is called skewness. The symmetry of the skew description is the relative mean, and whether the

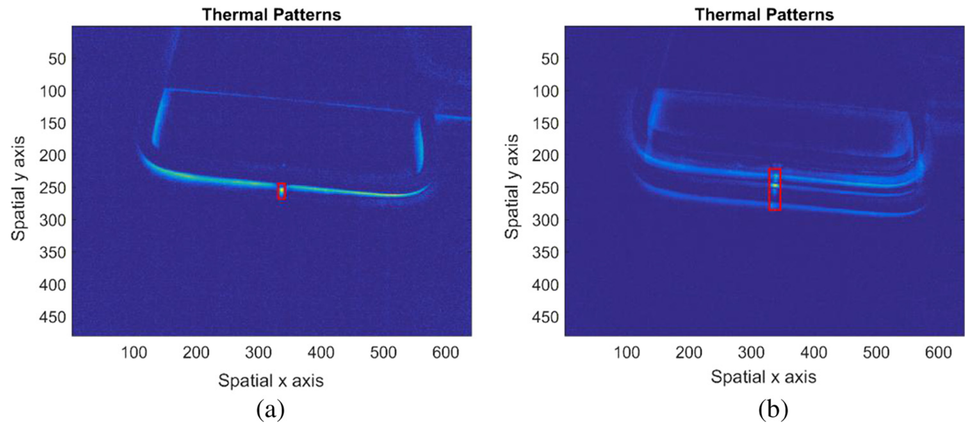

Fig. 7. (a) Feature which contains the most effective pixels in Fig. 5, (b) fusion image by the proposed method.

probability density distribution curve is symmetrical with respect to the mean.

Through the experiment studies, it is found that the effect of COBE method of image fusion can get a better result when the selected ICA features who has the second largest skewness. Give sample (a) as an example. The features extracted by ICA are shown in Fig. 8. The skewness of Feature 1, Feature 2, Feature 3 and Feature 4 is 13.0696, 3.0209, 2.1517 and 0.0786, respectively. It can be seen from the figure that the crack information is mainly concentrated on Feature 2 of ICA and this directly related to the second largest absolute value of skewness. Thus, this characteristic can be used as automatic feature selection of the fusion strategy.

In order to conduct proper validation, the signal-to-noise ratio (SNR) will be used for comparison, namely:

$$SNR = 10\lg\left(\sum_{i=1}^{m}\sum_{j=1}^{n}\mathbf{T}_{cij}^{2} \Big/ \sum_{i=1}^{m}\sum_{j=1}^{n}\mathbf{T}_{nij}^{2}\right) \tag{11}$$

where m represents the length of selected matrix, n represents the width of selected matrix, $\mathbf{T}_c$ represents the source region, $\mathbf{T}_n$ represents the noise region.

The proposed algorithm will be compared with Linear weighting and Skewness based fusion models. All of the experiments are applied by 4-steps directional scanning and each step of the thermal video extracts four features by using ICA.

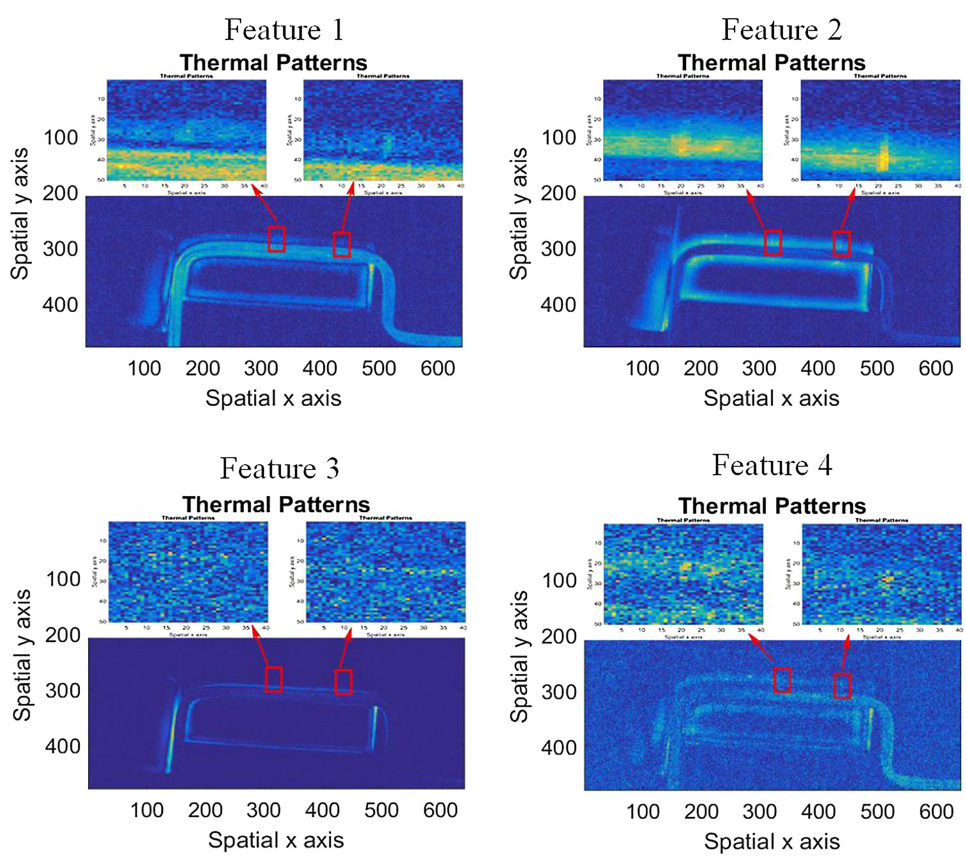

Fig. 8. Sample features extracted by ICA using skewness.

It can be seen from the Fig. 8, the linear weighting method is influenced largely by the moving distance of each step. When the coil is moving at a relatively small distance, no feature extraction is performed. The pixel fusion is made, and the noise generated by the coil is dense, which will directly affect the extraction of defects. In comparison, it can be seen clearly that the benefits of feature extraction by ICA enable us to separate the noise and crack information about high accuracy.

For sample (a) and sample (d), they are both based on dealing with a single crack (in order to verify the results of a single crack treatment of natural and artificial cracks, only parts of sample(a) are intercepted to compare the results). As is shown in Figs. 9 and 10, the red border represents the crack area and the white border represents the noise area (crack area is obtained by prior information, in order to ensure that two areas have almost the same noise, the noise area is selected nearest to the crack area), the same in following figures. According to Fig. 6, it can be seen that the extracted features by ICA basically do not contain the entire crack information. After the fusion, the proposed method can completely reconstruct defect profile. Table 3 gives the signal-to-noise ratio between the crack and the background noise.

Table 3 shows the comparison of SNR values of various fusion methods. The linear weighting method gives SNR results of 2.5931 dB and 7.4096 dB for sample (a) and sample (d). The value of the skewness method is roughly the same as the linear weighting method while genetic algorithm gives SNR result of 9.3919 dB and 18.0033 dB. Its value is three times as big as the linear weighting method and the skewness method. The result indicates that the proposed method has a significant performance improvement.

For sample (b), as is shown in Fig. 11, this is the case where the fusion algorithms deal with multiple cracks. Due to the large size of this sample, the distance between each step is relatively remote. Table 4 gives the signal-to-noise ratio between the crack and the background noise.

Table 4 shows the fusion methods of multi-crack detection. The linear weighting method gives a mean SNR results of 3.7985 dB, the mean SNR values of the genetic algorithm and the skewness method are roughly the same. The value is approximately twice as big as the linear weighting. Linear weighting is greatly influenced by noise. In position 5, genetic algorithm and skewness method have a better effect. However, the SNR value of linear weighting is less than 0 and the defect signal is weaker than the noise signal in which this greatly makes the difficulty of locating all the cracks. It can be seen that although the genetic algorithm and the skewness method both select the features separated by ICA, the defect information for different locations is significantly different. In contrast to the skewness method, the overall noise of genetic algorithm is smaller in the fused image.

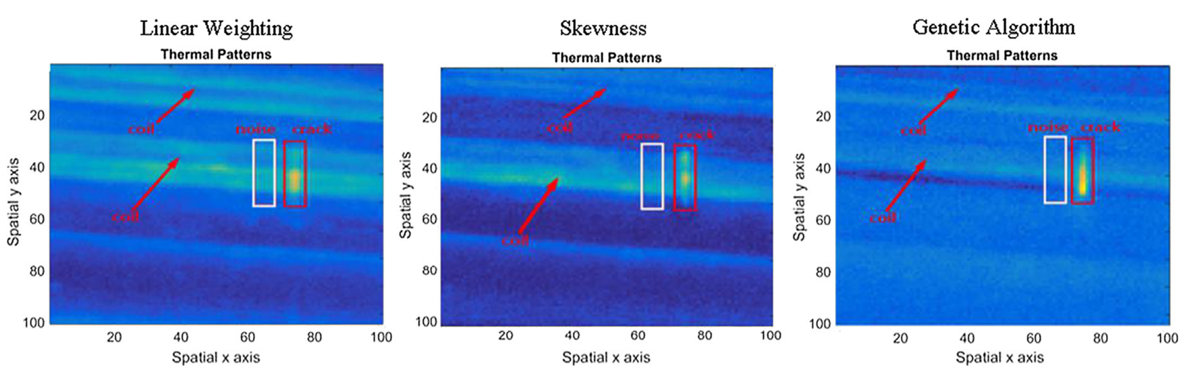

Fig. 9. Fusion images are obtained by three methods for sample (a).

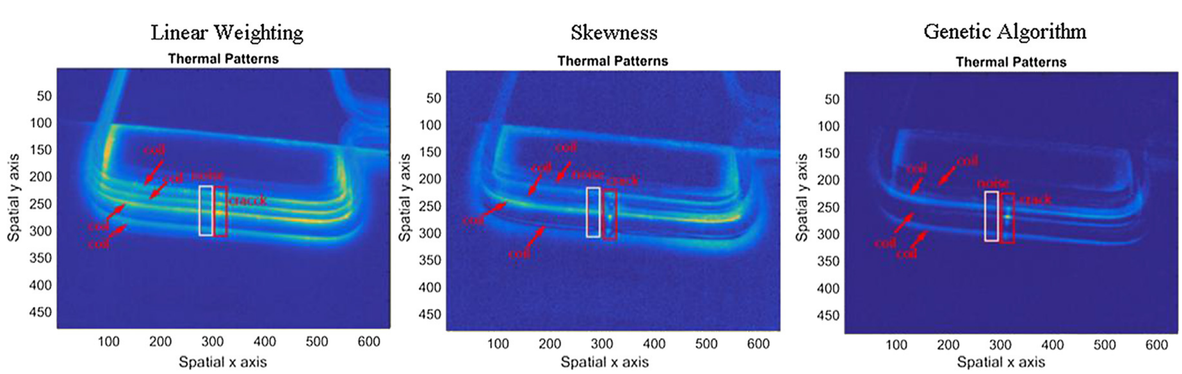

Fig. 10. Fusion images are obtained by three methods for sample (d).

Table 3
SNR of directional scanning ECPT system of sample (a) and sample (d).

Method	Sample (a)	Sample (d)	Compared with genetic algorithm	
			Sample (a)	Sample (d)
Linear weighting	2.5931	7.4096	6.7988	10.5937
Skewness	3.7533	6.5858	5.6386	11.4175
Genetic algorithm	9.3919	18.0033	0	0

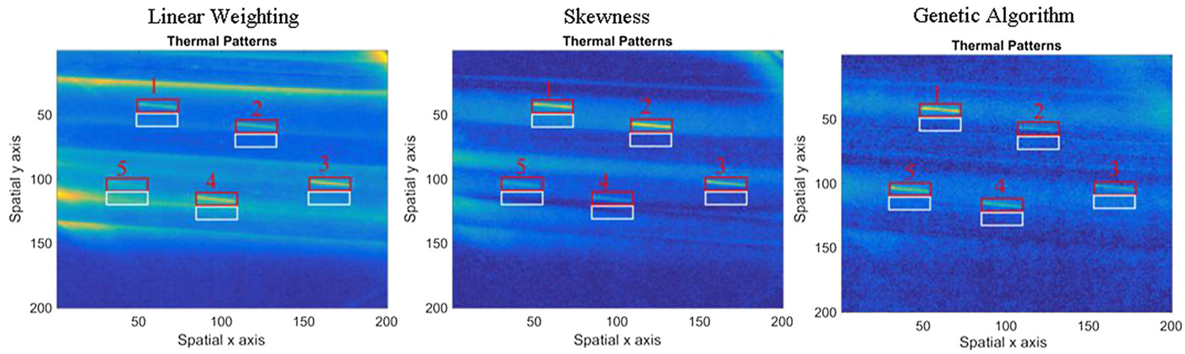

Fig. 11. Fusion images are obtained by three methods for sample (b).

Table 4
SNR of directional scanning ECPT system of sample (b).

Method	Cracks location of sample (b)					Average	Compared with genetic algorithm
	Position 1	Position 2	Position 3	Position 4	Position 5		
Linear weighting	6.8092	4.6544	6.1737	2.1607	−0.8054	3.7985	2.6504
Skewness	4.9220	8.0266	9.8409	6.9204	5.3988	7.0217	−0.5728
Genetic algorithm	8.6120	6.8466	1.9355	7.9329	6.9178	6.4489	0

For sample (c), as is shown in Fig. 12, this is the case where the fusion algorithms deal with different angle cracks. Since the size of the angle between the crack and the coil will affect the thermal pattern [33], Table 5 shows the SNR performance for the fusion algorithms at different angles.

Table 5 shows the fusion methods for different angle cracks. The average SNR values of the linear weighting method, the skewness method and the genetic algorithm are 7.1340 dB, 2.5858 dB and 4.3908 dB, respectively. The effect of the genetic algorithm is better than the skewness method and the linear weighting method works the best. For multi-angle cracks, the fusion effect for the larger angle crack and the smaller angle crack is better, whereas the effect of middle angle cracks is poor. The result of the fusion image is different from the conventional result (when the angle between coil and crack is in the range of 0–90°, the larger the angle is, the better the SNR effects are). There are many factors that affect the fusion results, including selected features extracted by the ICA of each step, the relative position of the coil and the defects, the relative position of each defect and so on.

The reason why the SNR for middle angle cracks is poorer than the larger and smaller angle cracks is that the coil in the first step and the second step is very close to 0°angle crack, it will result in high SNR. In this crack, this can be seen from the linear weighting method since the later is actually the average temperature as the coil move. The reason for the different result between the skewness method and other methods is the strategy of feature selection. The process of skewness method is to find out the larger SNR feature for all the cracks in each step. However, the process of genetic algorithm is to find more obvious cracks. Specifically, take sample (c) as an example, after features extraction of the video of each step

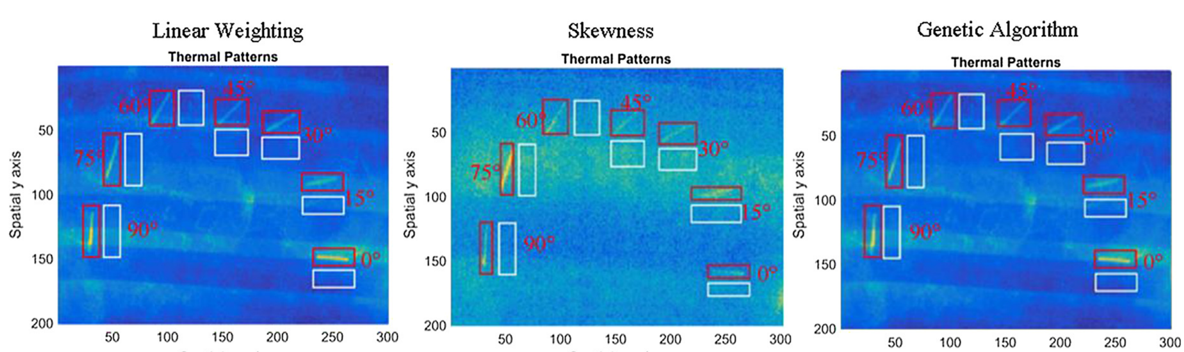

Fig. 12. Fusion images are obtained by three methods for sample (c).

Table 5
SNR of directional scanning ECPT system of sample (c).

Method	Multi-angle cracks of sample (c)							Average	Compared with genetic algorithm
	0°	15°	30°	45°	60°	75°	90°		
Linear weighting	11.8307	4.7178	5.4947	3.9785	5.1782	11.5624	7.1759	7.1340	−2.7432
Skewness	1.2097	2.5361	1.1423	0.8534	1.1429	7.9458	3.2706	2.5858	1.8050
Genetic algorithm	7.2994	5.2119	2.0168	1.8788	2.5222	9.2116	5.1173	4.3908	0

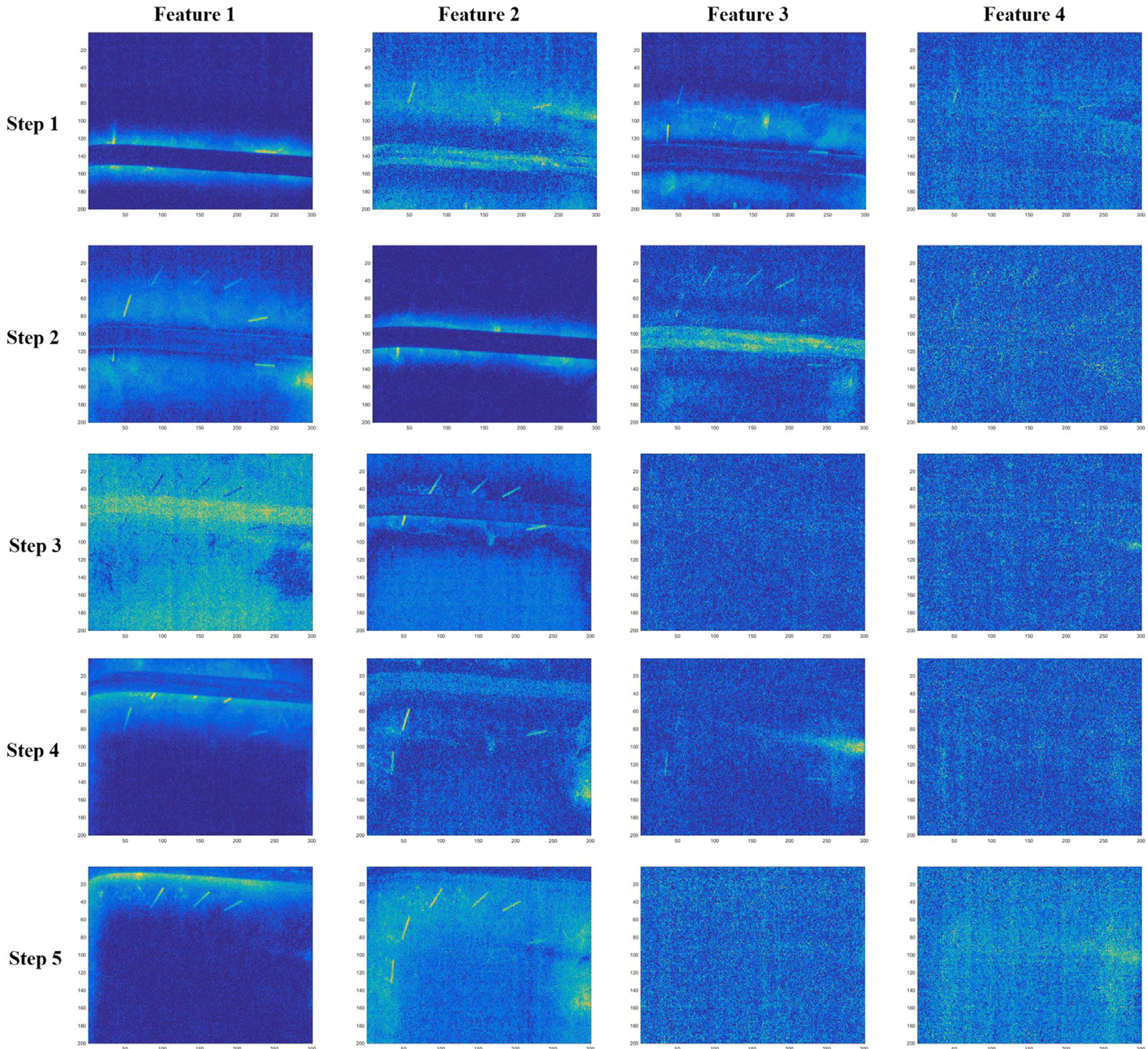

Fig. 13. All features extracted by ICA for sample (b).

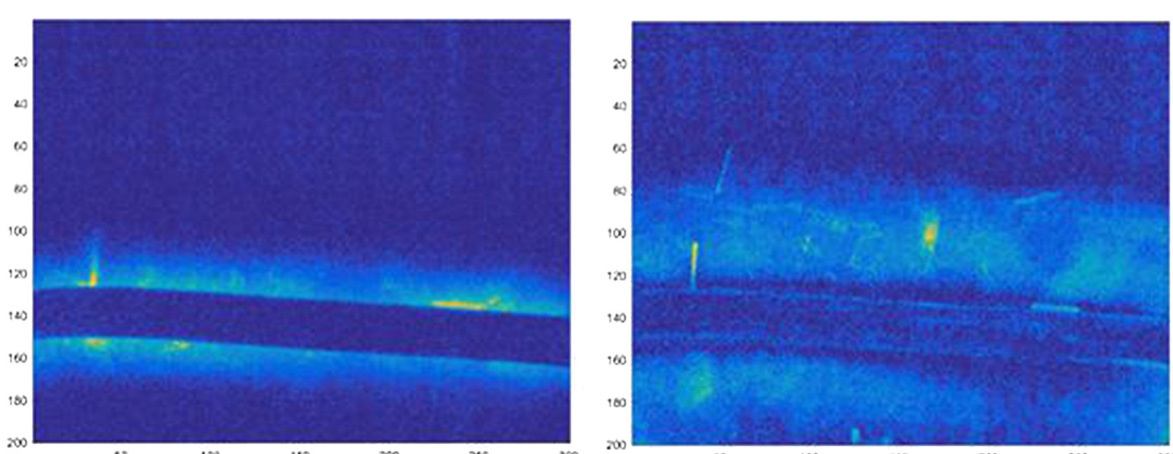

Fig. 14. Corresponding to Feature 1 and Feature 3 in step 1 of Fig. 9.

in Fig. 13, the skewness method selects the features in the videos for each step as 3,1,1,3,1 respectively. However, the genetic algorithm method selects the features in the videos for each step as 1,1,2,3,1 respectively. The difference lies in step 1 and step 3. Because the main concern of genetic algorithm is the point of strong information, it can be seen in Fig. 14 that feature 1 of step 1 has a very high crack information at 0°angle crack and 90°angle crack whereas it is difficult to see any information at 15°angle crack and 75°angle crack. The skewness algorithm takes a compromise, we can see the flaw information at four angles, but it has

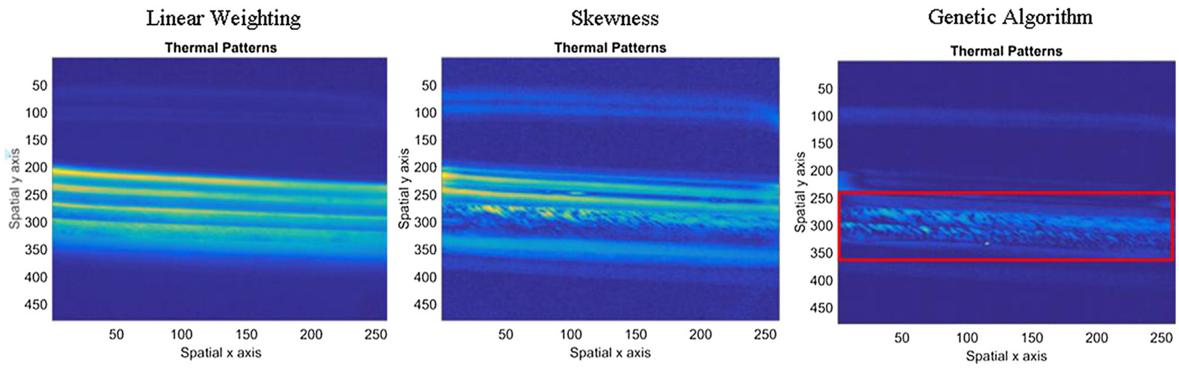

Fig. 15. Fusion images are obtained by three methods for sample (e).

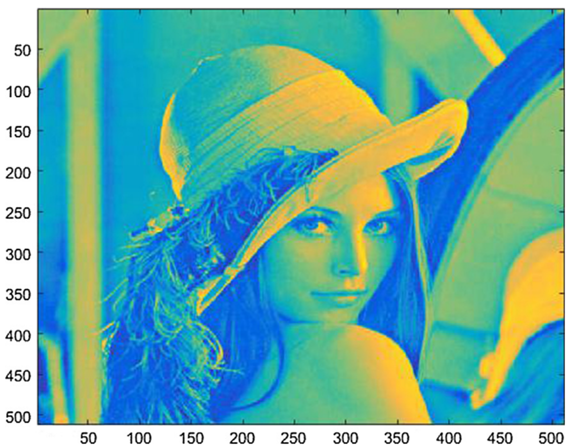

Fig. 16. Pseudo color image of lena.

poor SNR for feature 1 at 0°angle crack and 90°angle crack. This explains why the SNR for middle angle cracks is poor than the larger and smaller angle cracks and why the skewness method is not affected by the angle of cracks.

For sample (e), it can be seen in Fig. 15, this is the case where the fusion algorithms deal with multiple natural cracks. Accidents occur frequently because of natural cracks at the rails. Safety inspection of tracks is critical and natural cracks can be visualized clearly by using the proposed method whereas the linear weighting method produces big ambiguities. Since the linear weighting method does not carry out the process of feature extraction, this inevitably results in more interference from the background and noise. Because of these uncertainties, we call it "ambiguities". The heat transfer process is smooth on the conductor, and only in the event of a defect or edge will produce heat accumulation. It will render the defect area with a clear temperature difference compared to the adjacent area. In Fig. 15, the curved, thin and bright area is detected crack in the red box. The cracks which are

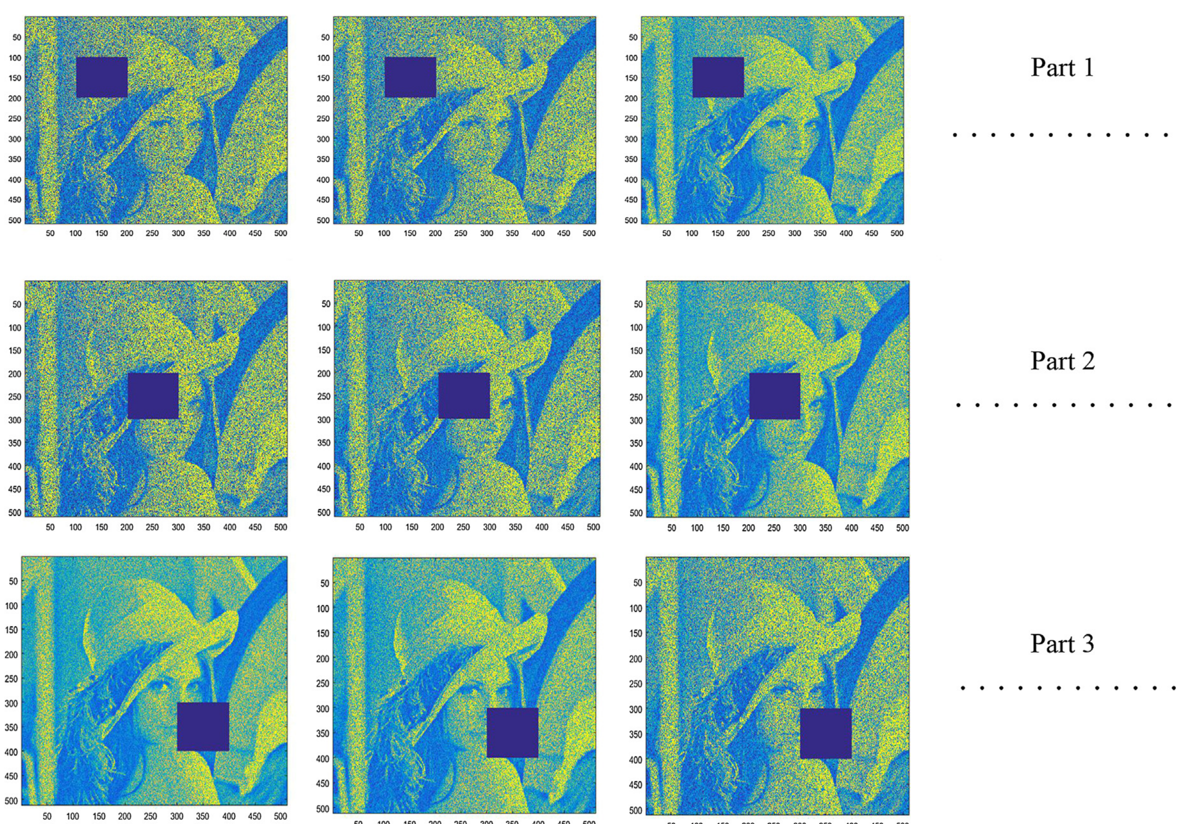

Fig. 17. Images from each part of proposed method.

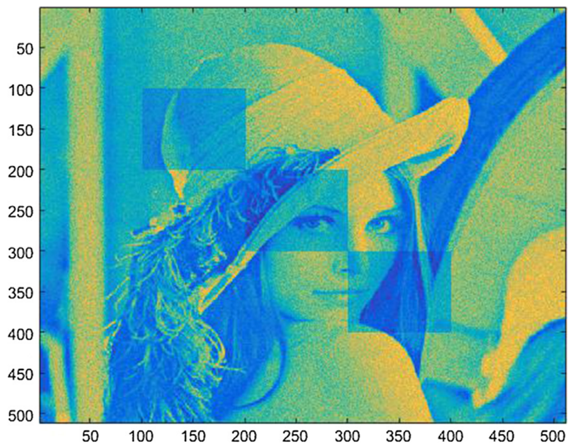

Fig. 18. Fusion result by Genetic algorithm.

got by genetic algorithm here are more obvious than the other methods.

The method proposed in this paper not only applies to ECPT system, it also has some achievements for other multi-step video information enhancement. Take lena image for example in Fig. 16, its size is 512 × 512. We get 30 copies of this image, each image adds a different ratio of speckle noise, then divides them into 3 parts. Each part has 10 images and adds a certain blocked area, as shown in Fig. 17.

By minimizing the cost function of information entropy, the fusion result is shown in Fig. 18.

In overall comparison, the method that inheriting the most information is the linear weighting method. It also produces the strongest noise. Both skewness method and the proposed method select the features of ICA extraction and the overall effect of the proposed method is obviously better than the skewness method. This is confirmed especially in dealing with the case sample of a single crack.

4. Conclusion and future work

In this paper, a spatial-time-state fusion method has been proposed to deal with the problem of defect location without knowing prior information. Both state ECPT system and algorithm have been validated. Through ICA for multi-step features extraction, as well as the hybrid of genetic algorithm and COBE, the defect image can be completely reconstructed. Finally, the location of defects is determined automatically by selection of the abnormal pattern of the fused image. The SNR is introduced to verify the robustness of the results. The proposed method has been tested on both man-made and natural defects from industry. Future work will focus on better features extraction methods which can completely separate the defects and noise as far as possible, and defects detection of objects under certain speed.

Acknowledgement

The work was supported by National Natural Science Foundation of China (Nos. 61401071, 61527803), Supported by NSAF (Grant No. U1430115) and EPSRC IAA Phase 2 funded project: "3D super-fast and portable eddy current pulsed thermography for railway inspection" (EP/K503885/1).

References

[1] R. Halmshaw, Non-destructive testing. Arnold, 1991.
[2] A. Adriaens, Non-destructive analysis and testing of museum objects: an overview of 5 years of research, Spectrochim. Acta Part B: Atomic Spectrosc. 60 (12) (2005) 1503–1516.
[3] W.M. Ayers, Non-destructive testing method: U.S. Patent 3,555,881. 1971-1-19.
[4] J. Blitz, Electrical and magnetic methods of non-destructive testing, Springer Science & Business Media, 2012.
[5] C.J. Hellier, Key elements of magnetic particle testing: magnetic particle examination is a very effective nondestructive examination method for the detection of surface and near surface discontinuities, Quality 54 (8) (2015), S8 S8.
[6] B. Mehta, Surface and subsurface crack analysis in carbon steel samples using magnetic particle testing and liquid penetrant testing, Mater. Evaluation, 2015, 73(4).
[7] S.P. Farrell, M. Lugg, K. Avery, Application of alternating current field measurement for determination of surface cracks and welds in steel structures at lift-off, in: ASNT 24th Research Symposium 2015. 2015, pp. 24–28.
[8] Masashi Ishikawa, Hiroshi Hatta, Yoshio Habuka, Ryo Fukui, Shin Utsunomiya, Detecting deeper defects using pulse phase thermography, Infrared Phys. Technol. 57(2) 2013 42–49.
[9] N.P. Avdelidis, B.C. Hawtin, D.P. Almond, Transient thermography in the assessment of defects of aircraft composites, NDT&E Int. 36 (2003) 433–439.
[10] S. Marinetti, E. Grinzato, P.G. Bison, E. Bozzi, M. Chimenti, G. Pieri, O. Salvetti, Statistical analysis of IR thermographic sequences by PCA, Infrared Phys. Technol. 46 (2004) 85–91.
[11] M. Pan, Y. He, G. Tian, et al., Defect characterisation using pulsed eddy current thermography under transmission mode and NDT applications, Ndt E Int. 52 (2012) 28–36.
[12] L. Cheng, G.Y. Tian, Surface crack detection for carbon fiber reinforced plastic (CFRP) materials using pulsed eddy current thermography, IEEE Sens. J. 11 (12) (2011) 3261–3268.
[13] N.P. Avdelidis, B.C. Hawtin, D.P. Almond, Transient thermography in the assessment of defects of aircraft composites, Ndt E Int. 36 (6) (2003) 433–439.
[14] L. Cheng, B. Gao, G.Y. Tian, et al., Impact damage detection and identification using eddy current pulsed thermography through integration of PCA and ICA, IEEE Sens. J. 14 (5) (2014) 1655–1663.
[15] N. Cvejic, D.R. Bull, N. Canagarajah, Regionbased multimodal image fusion using ICA bases, IEEE Sens. J. 7 (5) (2007) 743–751.
[16] L. Bai, B. Gao, G.Y. Tian, W.L. Woo, Y. Cheng, Spatial and time patterns extraction of eddy current pulsed thermography using blind source separation, IEEE Sens. J. 13 (6) (Jun. 2013) 2094–2101.
[17] Bin Gao, Libing Bai, Gui Yun Tian, W.L. Woo, Yuhua Cheng, Automatic defect identification of eddy current pulsed thermography using single channel blind source separation, IEEE Trans. Instrum. Meas. 63 (4) (2014) 913e922.
[18] J. Yang, X. Zhang, Feature-level fusion of fingerprint and finger-vein for personal identification, Pattern Recogn. Lett. 33 (5) (2012) 623–628.
[19] G. Zhou, A. Cichocki, Y. Zhang, et al., Group component analysis for multiblock data: common and individual feature extraction, IEEE Trans. Neural Networks Learn. Syst. 27 (11) (2016) 2426–2439.
[20] L Gao, L Qi, E Chen, et al., Discriminative multiple canonical correlation analysis for multi-feature information fusion, in: Multimedia (ISM), 2012 IEEE International Symposium on. IEEE, 2012, pp. 36–43.
[21] R. Ibrahim, J. Alirezaie, P. Babyn, Pixel level jointed sparse representation with RPCA image fusion algorithm, in: Telecommunications and Signal Processing (TSP), 2015 38th International Conference on. IEEE, 2015, pp. 592–595.
[22] Jäckel, Patrick, et al., The influence of external magnetic fields on crack contrast in magnetic steel detected by induction thermography, Quantitative InfraRed Thermogr. J. 10.2 (2013) 237–247.
[23] B Gao, A Yin, Y Wang, et al., Thermography spatial-transient-stage tensor model and materal property characterization, in: Nondestructive Evaluation/ Testing (FENDT), 2014 IEEE Far East Forum on. IEEE, 2014, pp. 199–203.
[24] J. Wilson, G.Y. Tian, I.Z. Abidin, S. Yang, D. Almond, Modelling and evaluation of eddy current stimulated thermography, Nondestr. Test. Eval. 25 (3) (2010) 205–218.
[25] B. Gao, L. Bai, W.L. Woo, G.Y. Tian, Y. Cheng, Automatic defect identification of eddy current pulsed thermography using single channel blind source separation, IEEE Trans. Instrum. Meas. 63 (4) (Apr. 2014) 913–922.
[26] S. Marinetti et al., Statistical analysis of IR thermographic sequences by PCA, Infr. Phys. Technol. 46 (1) (2004) 85–91.
[27] J.H. Holland, Genetic algorithms, Scientific American, 267(1) (1992) 66–72; Q Sun, S.G. Zeng, P.A. Heng, et al., The theory of canonical correlation analysis and its application to feature fusion. Chin. J. Comput.-Chin. Ed.-, 28(9) (2005) 1524.
[28] G. Vértesy, I. Tomáš, I. Mészáros, Non-destructive indication of plastic deformation of cold-rolled stainless steel by magnetic adaptive testing, J. Magnet. Magnetic Mater. 310 (1) (2007) 76–82.
[29] I. Tomas, Non-destructive magnetic adaptive testing of ferromagnetic materials, J. Magnet. Magnetic Mater. 268 (1) (2004) 178–185.
[30] Q. Sun, S.G. Zeng, P.A. Heng, et al., The theory of canonical correlation analysis and its application to feature fusion, Chin. J. Comput.-Chin. Ed.- 28 (9) (2005) 1524.
[31] N. Tsopelas, N.J. Siakavellas, Performance of circular and square coils in electromagnetic–thermal non-destructive inspection, NDT E Int. 40 (1) (2007) 12–28.
[32] Y. He, R. Yang, Eddy current volume heating thermography and phase analysis for imaging characterization of interface delamination in CFRP, IEEE Trans. Ind. Inf. 11 (6) (Dec. 2015) 1287–1297.
[33] I.Z. Abidin, G.Y. Tian, J. Wilson, et al., Quantitative evaluation of angular defects by pulsed eddy current thermography, Ndt E Int. 43 (7) (2010) 537–546.